IEEE Access
Multidisciplinary | Rapid Review | Open Access Journal

IEEE ENGINEERING IN MEDICINE AND BIOLOGY SOCIETY SECTION

Received 31 October 2023, accepted 7 December 2023, date of publication 14 December 2023,
date of current version 21 December 2023.

Digital Object Identifier 10.1109/ACCESS.2023.3342917

APPLIED RESEARCH

Classification of Alzheimer's Disease Using Ensemble Convolutional Neural Network With LFA Algorithm

CHANG-MIN KIM[1] AND WOOBEOM LEE[2]

[1]AI Software Education Institute, Soonchunhyang University, Asan-si 31538, South Korea
[2]Department of Information Communication Software Engineering, Sangji University, Wonju-si 26339, South Korea

Corresponding author: Woobeom Lee (beomlee@sangji.ac.kr)

This work was supported in part by the Regional Innovation Strategy (RIS) through the National Research Foundation of Korea (NRF) funded by the Ministry of Education (MOE), in 2023, under Grant 2022RIS-005; and in part by the Soonchunhyang University Research Fund under Grant 20230663.

ABSTRACT Alzheimer's disease (AD) is a disease that develops gradually, ultimately causing deterioration of brain functions. Thus, early diagnosis is essential for treating and managing AD. Magnetic-resonance-imaging (MRI)-based AD diagnosis classifies the stage of AD according to the extent of atrophy caused to a patient's hippocampal and entorhinal cortex. In this case, the shape of the patient's brain serves as a crucial feature. Therefore, in this paper, we propose an ensemble convolutional neural network (CNN) model that can classify the AD stage according to the shape of a patient's brain. The proposed model is structured by combining a convolutional layer part of the visual geometry group network (VGGNet) model, with proven performance in image classification, and a 1D CNN model into a pipeline. Here, the 1D CNN applies the line segment feature analysis (LFA) algorithm to MRI images to transform the visual line segment information of the images into vectors and record strong features indicating the shape of the brain. This is followed by 1D CNN model training. Notably, the 1D CNN model can carefully observe the brain shape owing to the parallel connection of ten 1D convolutional layers with LFA features. Subsequently, the brain shape information is combined with features obtained from the original image through the VGGNet to improve the model performance compared to that of existing methods. To evaluate the performance of the proposed ensemble CNN model, MRI datasets collected from Kaggle are used to evaluate and compare the proposed model with existing image classification methods and methods proposed in related studies. The experimental results reveal that the proposed model demonstrates superior performance with an accuracy of 0.986 and a loss of 0.0385.

INDEX TERMS Alzheimer's disease, ensemble convolution neural network, VGGNet, 1D convolution neural network, brain MRI, LFA algorithm.

I. INTRODUCTION

Alzheimer's disease (AD) is a degenerative brain disease first reported in 1907 by a German psychiatrist, Alois Alzheimer, and it is characterized by an extremely slow onset and gradual progression [1], [2], [3]. Related studies have discovered that the onset of AD can be attributed to the deposition of excessively produced beta-amyloid in the brain or brain cell damage, such as hyperphosphorylation of tau proteins, inflammatory response, and oxidative damage [4], [5]. In the early stages of AD, patients develop memory-related problems, and as the disease progresses, AD patients exhibit abnormalities in various other cognitive functions, such as language functions and decision-making capability, leading to dementia. Hence, AD is among the most dangerous diseases.

Dementia affects more than 55 million people globally, with nearly 10 million new cases annually [6]. Predictions indicate that the dementia patient count will rise to 152.8 million by 2050 [7]. China accounts for a quarter of

The associate editor coordinating the review of this manuscript and approving it for publication was Alessandra Bertoldo.

the worldwide dementia population, with about 15.07 million patients aged 60 and above [8]. Alzheimer's disease (AD) and other forms of dementia are becoming pressing public health and societal concerns.

Different countries and regions display varying rates of AD diagnosis, prevalence of dementia, and mortality due to social, economic, and demographic factors. A systematic review in 2020 revealed higher dementia prevalence in Europe and North America compared to South America, Asia, and Africa [9]. Thanks to enhancements in education, reduced vascular risk factors, and a decrease in stroke incidence [10], [11], [12], [13], the prevalence of AD and dementia has decreased in Europe and the U.S. [10], [14], [15], [16], [17]. However, due to an aging population, mortality rates for AD and dementia are expected to rise. In the U.S., there were 121,499 recorded deaths related to AD in 2019 [18]. CDC data shows an AD mortality rate of 37 per 100,000 individuals, ranking it as the 6th leading cause of death. COVID-19 has increased dementia-related deaths by 16% [19]. In the UK, the dementia-related mortality rate in 2019 was 115.1 per 100,000 (66,424 deaths), lower than 123.8 (69,478 deaths) in 2018. Nevertheless, COVID-19 disproportionately affected dementia patients, leading to death rates 8 times higher [20], [21]. Asia witnesses a rapid rise in the elderly population. Japan, a super-aged society, is expected to have 6.5 to 7 million AD patients by 2025 and 8.5 to 11.5 million by 2060 [22]. Japan's dementia mortality rose from 15.3 per 100,000 in 1999 to 69.0 in 2016 [23]. South Korea faces increased prevalence and mortality due to an aging population and low birth rates. Dementia cases in Koreans aged 60+ were 135,630 in 2003 and 269,631 in 2015. Mortality increased 2.5 times from 2009 to 2019, elevating it from 13th to 7th leading cause of death [24]. China's dementia prevalence rates for those aged 60+ are 6.0% (total dementia), 3.9% (AD), 1.6% (vascular dementia), and 0.5% (other dementias). China's AD and dementia mortality rates in 2019 were 22.5 per 100,000, rising since 1990 and moving from 10th to 5th leading cause of death [25].

The World Health Organization (WHO) also anticipates that 114 million people out of the global population will be patients by 2050. Hence, the WHO has recommended governments and policymakers to consider dementia as a high-priority global public health problem [26], [27], [28]. According to the 2021 cause-of-death statistics report released by Statistics Korea in September 2022, the mortality rate associated with AD has increased from 4.8% to 15.6% in the dementia mortality trend from 2011 to 2021 in the Republic of Korea [29]. Therefore, care management cost for dementia patients is expected to increase by approximately eight times to 106.5 trillion won (approximately 3.8% of the GDP) by 2050 [29].

Because the cause and treatment of AD remain unclear to date, detecting the onset of AD in early stages is crucial [30]. This is because early detection can prevent the worst case, which is the progression of AD into dementia. Furthermore, establishing a rapid treatment plan based on the progress of the disease and continuous care management may be feasible.

Compared to magnetic resonance imaging (MRI) images of normal brains, the hippocampal and entorhinal cortex appear atrophied in the MRI brain images of AD patients. In particular, a clear difference can be observed in the hippocampal region [30]. These characteristics enable early diagnosis of AD and can help in monitoring and tracking the progress of the disease by detecting atrophy in the hippocampal region of the MRI brain images of AD patients.

In this study, we classified the stage of AD into the following four categories: ''Non-Demented,'' ''Very Mild Demented,'' ''Mild Demented,'' and ''Moderate Demented,'' according to the extent of atrophy observed in the hippocampal and entorhinal cortex in MRI images. To extract the most important contour information from MRI images when diagnosing AD, the line segment feature analysis (LFA) algorithm [31], [32], [33] was used to analyze the features of contour shapes. In addition, an ensemble convolutional neural network (CNN) model was constructed by combining a 1D CNN model with the visual geometry group network (VGGNet) model. The ensemble CNN model was then used to classify AD.

In a previous study on AD diagnosis, Hosseini-Asl et al. constructed the upper layer of a 3D CNN with a 3D convolution autoencoder to detect the brain size, ventricle size, and hippocampus biomarkers. The authors then classified target domains [34]. This 3D CNN used parallel convolutional layers to extract various biomarkers from a single input. Consequently, a memory unit with high specifications was required when working with high-resolution images, such as MRI images. Furthermore, a high-performance server had to be used for hierarchical MRI images. Venugopalan et al. constructed a deep learning model with connected shallow neural structures for early diagnosis of AD. The authors integrated and used MRI, single nucleotide polymorphisms, and clinical test data [35]. As a method for automatic classification of AD stages and mild cognitive impairment, Basaia et al. diagnosed AD by conducting experiments considering various classification criteria using an all-convolutional network model trained on the Alzheimer's Disease Neuroimaging Initiative dataset and the Milan dataset collected by the authors [36]. Murugan et al. proposed a DEMentia NETwork (DEMNET) model consisting of 14 layers using a block that grouped the convolution, batch-norm, and max-pooling layers to identify the stage of AD progression [37].

In this study, global biomarkers were extracted from MRI images using the VGGnet model, which uses unprocessed MRI image data. In addition, the LFA algorithm was used to extract strong morphological features of the brain shape from MRI images. Minute local biomarkers were then extracted using a 1D CNN model to improve performance in AD diagnosis. Moreover, by utilizing the LFA algorithm to transform the image data into vector signals, we developed a method different from existing CNN-based diagnosis methods that require additional structured or time-series data.

II. RELATED RESEARCH

A. STRUCTURE OF VGGNet

The VGGNet is a model with a deep hierarchical structure that presents superior performance, and it ranked second in the ImageNet Large Scale Visual Recognition Challenge 2014 (ILSVRC 2014) [38]. This model uses consecutive 3 × 3 filters and is classified as a VGG16 or VGG19 model depending on the number of layers in the model. As the number of layers in the model increases, the performance of the model improves. However, problems such as overfitting and gradient vanishing persist. Thus, the decision function of input data is constructed in the VGGNet by overlapping a small 3 × 3 convolution filter using the rectified linear unit (ReLU) function. Furthermore, the extent of overfitting is reduced by decreasing the number of parameters in the learning process. Hence, the VGGNet maintains a stable learning process, yielding superior performance.

In a medical imaging classification study using the VGGNet, S. Lu [39] proposes a novel method for diagnosing Cerebral Microbleeds (CMB). This method is based on VGG, ELM (Extreme Learning Machine), and the Gaussian Map Bat algorithm. VGG, a well-known Convolutional Neural Network (CNN) model, is utilized to extract features from brain MRI images. Instead of training VGG with the CMB dataset, a pretrained VGG is directly employed to generate image features. These features are then fed into ELM for training. ELM, a learning algorithm for Single Hidden Layer Feedforward Networks (SLFN), trains the network in just three steps without iterative backpropagation, offering fast convergence and excellent classification performance compared to traditional backpropagation. The generalization ability of ELM is further enhanced using the Gaussian Map Bat algorithm. By combining these successful components, our CMB diagnosis method achieves results surpassing state-of-the-art approaches. Hong et al. [40] proposed a method for recognizing numerous genetic syndromes in children using the VGG16 model. Anusri et al. [41] conducted a facial emotion recognition study using the VGG16 model for early diagnosis of Parkinson's disease. Helaly et al. [42] have developed an end-to-end framework for the early detection of Alzheimer's disease. This framework performs medical image classification for various stages of Alzheimer's disease at its initial phases (referred to as AD), utilizing a CNN-based approach to conduct multi-class classification for four AD stages, and binary classification between two AD stages. The proposed framework is composed of six stages: data collection, preprocessing, data augmentation, medical image classification, evaluation, and application. The dataset undergoes resampling and preprocessing, including processes like normalization, standardization, and resizing. Data augmentation involves techniques such as rotation and flipping to enhance the dataset, which is subsequently split into training, validation, and test sets. Medical image classification is carried out using a simple CNN architecture that handles both 2D and 3D structural brain MRI scans, along with a pre-trained VGG19 model. The performance of these two methods is evaluated using nine performance metrics. Ebrahim et al. [43] proposed an AD diagnosis method using magnetic resonance imaging (MRI). In this study, they employed the relatively simple yet well-known VGG16 architecture. VGG16 consists of 13 convolutional layers, 5 pooling layers, and two fully connected layers – one with ReLU activation and the other with Softmax activation. The input images have a fixed size of 64×64, with a kernel size of 3×3 and max-pooling performed over a 2 × 2 pixel window with a stride of 2. This enabled them to distinguish between Alzheimer's disease (AD) and Cognitively Normal (CN), demonstrating that even with a shallow architecture, effective results can be obtained for AD diagnosis using image data.

Thus, the VGGNet model is widely used in the medical imaging field owing to its superior performance. This study also utilizes the VGGNet to classify AD images. As summarized in Table 1, the VGGNet has a structure wherein one or more convolution layers are grouped. The inclusion of convolution layers indicated in bold in Table 1 determines whether the structure of the VGGNet model is of type VGG16 or VGG19. In this study, we use the VGGNet, which is widely utilized in medical image analysis, to extract unique biomarkers as the global features of AD images.

TABLE 1. Structure of VGG16&19; fsize: filter size, pad: padding, st: stride, act: activation function.

No.	ConvNet Configuration
1	Conv3-64, fsize: 3×3, pad: 1, st: 1, act: ReLU Conv3-64, fsize: 3×3, pad: 1, st: 1, act: ReLU Max-pool, 3×3, st: 2
2	Conv3-128, fsize: 3×3, pad: 1, st: 1, act: ReLU Conv3-128, fsize: 3×3, pad: 1, st: 1, act: ReLU Max-pool, 3×3, st: 2
3	Conv3-256, fsize: 3×3, pad: 1, st: 1, act: ReLU Conv3-256, fsize: 3×3, pad: 1, st: 1, act: ReLU Conv3-256, fsize: 3×3, pad: 1, st: 1, act: ReLU **Conv3-256, fsize: 3×3, pad: 1, st: 1, act: ReLU** Max-pool, 2×2, st: 2
4	Conv3-512, fsize: 3×3, pad: 1, st: 1, act: ReLU Conv3-512, fsize: 3×3, pad: 1, st: 1, act: ReLU Conv3-512, fsize: 3×3, pad: 1, st: 1, act: ReLU **Conv3-512, fsize: 3×3, pad: 1, st: 1, act: ReLU** Max-pool, 2×2, st: 2
5	Conv3-512, fsize: 3×3, pad: 1, st: 1, act: ReLU Conv3-512, fsize: 3×3, pad: 1, st: 1, act: ReLU Conv3-512, fsize: 3×3, pad: 1, st: 1, act: ReLU **Conv3-512, fsize: 3×3, pad: 1, st: 1, act: ReLU** Max-pool, 2×2, st: 2
6	FC-4096
7	FC-4096
8	FC-1000, soft-max

B. STRUCTURE OF AlexNet

AlexNet is a CNN-based deep learning architecture that won the ILSVRC (ImageNet Large Scale Visual Recognition

TABLE 2. Line-segment type depending on the activated rank of the detection-filter.; N-A: non-activity, P: point, H: horizontality, V: verticality, C: curve, D: diagonal, F: face, P-n: pattern-n.

TYPES OF LINES	PATTERN NUMBERS
N-A/P/H/V/D/F	0/1, 2, 4, 8, 16, 32, 64, 128/3, 6, 7, 96, 192, 224/9, 20, 40, 41, 144, 148/10, 18, 72, 80/255
C	11, 14, 15, 19, 21, 22, 23, 26, 27, 30, 31, 37, 42, 43, 46, 47, 59, 62, 63, 73, 74, 75, 79, 82, 84, 86, 87, 88, 91, 93, 94, 104, 105, 106, 107, 110, 111, 112, 115, 116, 118, 119, 120, 121, 122, 124, 125, 127, 133, 146, 147, 150, 151, 155, 158, 159, 161, 164, 186, 187, 190, 191, 200, 201, 203, 206, 207, 208, 210, 211, 212, 214, 215, 216, 217, 218, 220, 221, 223, 232, 233, 234, 235, 238, 239, 240, 242, 243, 244, 246, 247, 248, 249, 251, 252, 253, 254
P-1/P-2/P-3	5, 24, 33, 36, 66, 129, 132, 160/13, 25, 28, 35, 50, 56, 67, 70, 76, 97, 98, 134, 152, 168, 176, 194, 196/29, 99, 184, 198
P-4/P-5/P-6	12, 17, 34, 48, 65, 68, 130, 136/38, 44, 52, 100, 131, 137, 145, 193/39, 45, 135, 149, 169, 180, 225, 228
P-7/P-8/P-9	49, 69, 81, 138, 140, 162/51, 77, 85, 113, 142, 170, 178, 204/53, 58, 78, 83, 89, 92, 101, 114, 141, 154, 163, 166, 172, 177, 197, 202
P-10/P-11/P-12	54, 108, 139, 209/55, 109, 143, 171, 182, 213, 236, 241/57, 71, 156, 226
P-13/P-14/P-15	60, 102, 153, 195/61, 103, 157, 185, 188, 199, 227, 230/90, 165
P-16/P-17/P-18/P-19	95, 123, 175, 183, 222, 237, 245, 250/117, 174, 179, 205/126, 189, 219, 231/167, 173, 181, 229

Challenge) in 2012, surpassing VGGNet and making a significant impact on the field of image recognition [44]. AlexNet was capable of learning from the ImageNet dataset, which consists of over 1.2 million labeled images. It introduced the use of GPUs for parallel computation, greatly enhancing the training speed. In the 2012 ILSVRC, it secured first place with an error rate difference of about 10% from the second place, contributing significantly to the popularization and advancement of deep learning.

- **Input Layer:**AlexNet takes color images of size 224 × 224 as input.
- **Convolutional Layer:**AlexNet includes 5 convolutional layers, each extracting features using filters. The first convolutional layer uses 96 filters of size 11 × 11, while the subsequent layers use smaller filters.
- **Max-Pooling Layer:**Max-Pooling layers follow the convolutional layers, downsampling the image to reduce its size.
- **ReLU Activation:** ReLU (Rectified Linear Unit) activation functions are used between all convolutional layers and fully connected layers. ReLU adds non-linearity, enhancing the model's representational capacity.
- **Fully Connected Layer:** AlexNet has 3 fully connected layers that learn features and perform classification tasks.
- **Softmax Layer:** The output layer employs the Softmax activation function to compute class probabilities.

C. PROCESS OF LINE-SEGMENT FEATURE ANALYSIS (LFA)

Notably, AD is characterized by progressive changes in the shape of the brain owing to atrophy of the hippocampal and entorhinal cortex. In this study, we classify the progressive stages of AD by further emphasizing the characteristics of changes in the brain shape.

The LFA algorithm [31], [32], [33] is an algorithm proposed in our previous study. This algorithm can transform visual data into structured data by analyzing contour features, which are basic elements comprising the objects in images, as line segments in pixel units.

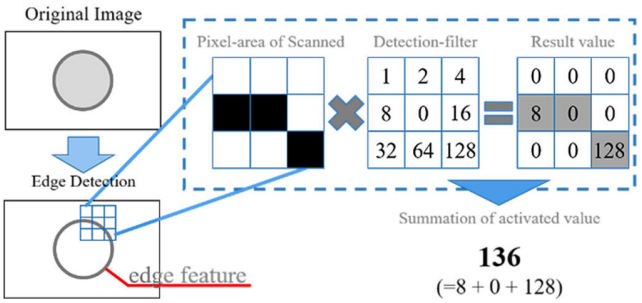

FIGURE 1. Example of the line-segment analysis process of the LFA algorithm.

Fig. 1 portrays a process whereby visual line segment data is transformed into structured numerical data using the LFA algorithm. In this process, all visual line segments within the input image are converted into a series of numerical patterns based on their contour type. The 3 × 3 detection filter employed in this process has a coefficient value of 2^n. Table 2 provides an overview of the line segment types that can be characterized using the detection filter. The detection filter can condense visual features by representing visual line segments with 256 unique numbers. By filtering the input image with the detection filter, line segments from the input image are portrayed through 256 distinct visual line segment attributes, determined by the filter response values as detailed in Table 2. These distinct identifiers are sorted by type and aggregated to generate LFA data, which functions as input for the 1D CNN.

The generated LFA data takes the form of a 256 × 1 vector, corresponding to the sum of the decision filter coefficients. The original image is segmented, and the LFA algorithm is applied to each segmented area to emphasize the overall shape features of the objects. Hence, if the original image is

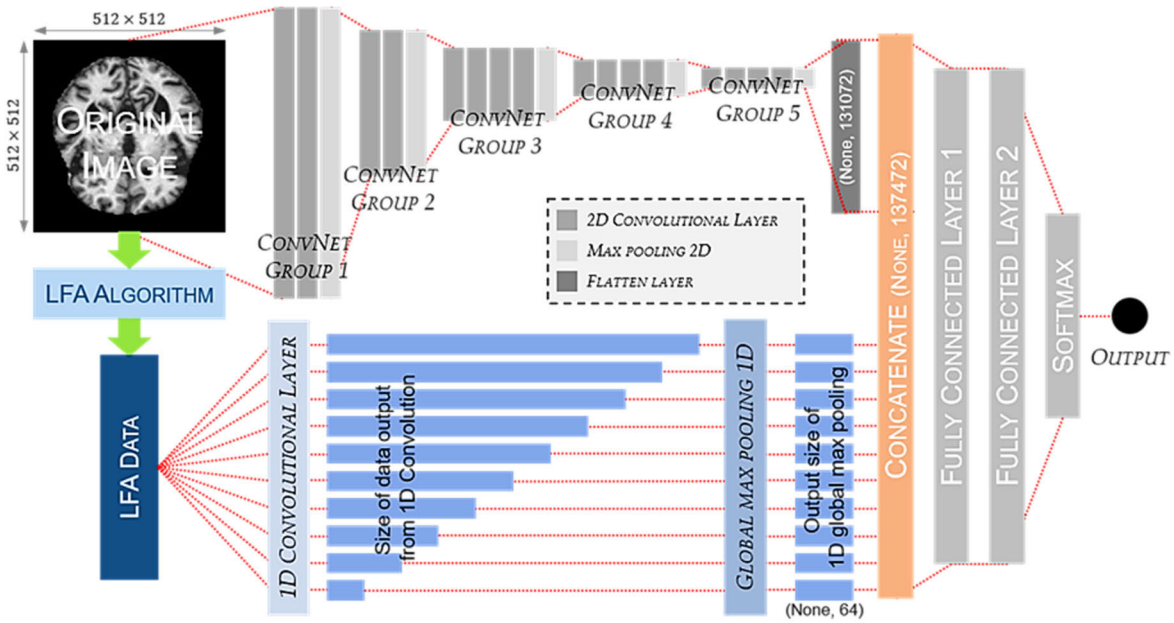

FIGURE 2. Proposed ensemble CNN model connected VGGNet and 1D-CNN with LFA.

segmented into an N × M size, the resultant LFA data will possess a size of N × M × 256 × 1.

The generated LFA data can emphasize line segments with the highest frequency according to the type of line segments contained in the image objects. For example, if a circular object is present in the image, similar to the original image displayed in Fig. 1, the values transformed through the detection filter will possess several unique numbers of line segment types representing curves and diagonal lines. Moreover, if these values are plotted on a graph by type, the curves and diagonal lines will have a high frequency.

This study aims to improve the performance of AD diagnosis by emphasizing detailed features of the brain shape, which are the strongest, using MRI images processed using the LFA algorithm.

D. 1D CONVOLUTIONAL NEURAL NETWORK

CNNs are typically designed to operate only on 2D or higher dimensional data, such as images and videos, through 2D or 3D convolutional layers in various computer vision and machine learning tasks [45], [46], [47], [48], [49]. However, as CNNs are used in wide-ranging applications, several studies are being conducted on learning methods for 1D data.

To learn time-series signal data, such as electrocardiogram signals, a 1D CNN is trained on the signal data using a 2D or higher dimensional kernel with a 1D form [50]. Therefore, 1D CNNs are considerably more efficient than 2D CNNs in terms of computational complexity [51]. Furthermore, 1D CNNs are advantageous in that they can be used effectively in hardware environments, such as small devices [52], [53], [54].

The 1D CNN model used in this study was trained on 1D data transformed through the LFA algorithm. Because the transformed data were generated by reducing visual features, comprehensively analyzing all data was meaningless. However, meaningful features could be obtained from the reduced data if the changes in the coefficients for each line segment type were analyzed. In particular, change relationships of consecutive values, such as time-series data, are important in the transformed data. Hence, these features were extracted through the 1D CNN model.

III. PROPOSED ENSEMBLE CNN MODEL FOR EARLY DIAGNOSIS OF ALZHEIMER'S DISEASE

In this paper, we propose an ensemble CNN model that integrates the VGGNet (using MRI images as the input) and 1D CNN (using the LFA data as the input) into a pipeline, as depicted in Fig. 2, for early AD diagnosis.

As indicated in Fig. 2, the proposed ensemble model is connected in parallel with convolutional layers No. 1 through No. 5, as in Table 1. The proposed ensemble model uses ten 1D convolution layers with different kernel sizes. The result value of each 1D convolution layer is combined with the result value of the VGGNet in the concatenate layer and integrated into a single input vector. The input vector is then passed through two fully connected layers and a softmax function to execute the final classification of the AD stage.

In general, 2D convolutional layers demonstrate excellent performance when recording spatial and directional information within an image. However, they present a drawback in that they encounter difficulties in analyzing the segmentation and contours of small regions. Therefore, the pipelines of two different models are connected to emphasize the advantages of the two models.

The LFA algorithm used to generate the input data of the 1D CNN cumulatively aggregates the visual line segment information from the image by contour type to express weak shape features as strong feature information. Furthermore, the visual line segment information from the image can be used as feature classification data through the 1D CNN connected in parallel. In particular, strong features for space and direction are collected through the 2D convolutional layers, and weak features are strengthened through the LFA and 1D CNN and transformed into strong features. This is followed by the collection of features corresponding to change relationships.

The VGGNet model used in this study uses the existing form defined in Table 1. In addition, the 1D CNN comprises ten parallel layers, as depicted in Fig. 2. Moreover, the i-th output neuron value, $Z^n_{i,k}$, in the k feature map of the 1D Conv-n, which is the n-th convolution layer of the 1D CNN, is computed using Equation (1) below.

$$Z^n_{i.k} = b^n_k + \sum_{u=0}^{f^n_s-1} \sum_{k'=0}^{f^n_m-1} x_{i'k'} \cdot W^n_{u,k} \tag{1}$$

where, $i' = i \times s_n + u$
s_n : *stride on* 1*D Conv* − *n*
b^n_k : *bias in* 1*D Conv* − *n*
f^n_s : *Filter size in* 1*D Conv* − *n*
f^n_m : *Number of feature map in* 1*D Conv* − *n*

In Equation (1), $x_{i'k'}$ denotes the output value of the i' position in the k feature map of the previous layer [50]. However, because the previous layer is not considered in this study, $x_{i'k'}$ represents the i' position in the LFA feature vector. b^n_k and $w^n_{u,k}$ denote the weight value and bias value of the u-th position in the filter of the k feature map of 1D Conv-n, respectively.

The 1D CNN used in this study consists of a single layer; thus, the use of padding is meaningless. In addition, the global max-pooling operation is applied to the value output obtained through the 1D convolution layer to collect the strongest features among the output features. The structure of each layer of the 1D CNN used in this study—in which 10 layers are connected in parallel—is configured as follows.

- **1D Conv-1:** The size of the kernel is 1 × 10, and the number of kernels is 32. The stride is set to one, ''ReLU'' is the activation function, and no padding is used.
- **1D Conv-2:** This layer is the second 1D convolutional layer connected in parallel, and it uses the same activation function, bias, and padding as 1D Conv-1. However, the kernel size is set to nine, and the stride is set to two.
- **1D Conv-3 ∼ Conv-10:**Parallel layers 3 to 10 have the same parameter settings as layers 1 and 2. Only the kernel size and stride are set differently, as indicated in Fig. 3. The kernel size is decreased by one, and the stride value is increased by one.

The CNN layers connected in parallel at the 1D CNN layer, which uses the LAF features as inputs, use different kernel sizes and strides. Hence, extracting various shape features is possible. A general CNN generates a feature map in which high-dimensional features are analyzed through deep processing, following which these features are classified through the fully connected layer. However, a high-dimensional analysis of visual features can be performed in the data generation process of LFA data obtained through the LFA algorithm. Specifically, because the LFA data are generated based on line segment information of the objects in the input image, they represent information with reinforced features of the object's shape. In addition, because the coefficients of the LFA input vector correspond to one unique line segment type, changes between the line segment types can be analyzed effectively. By designing the 1D CNN with a parallel structure, creating a feature map that extracts various detailed features using different parameters of each layer is possible. Consequently, the loss and damage of the feature data possibly occurring during the LFA generation process can be mitigated.

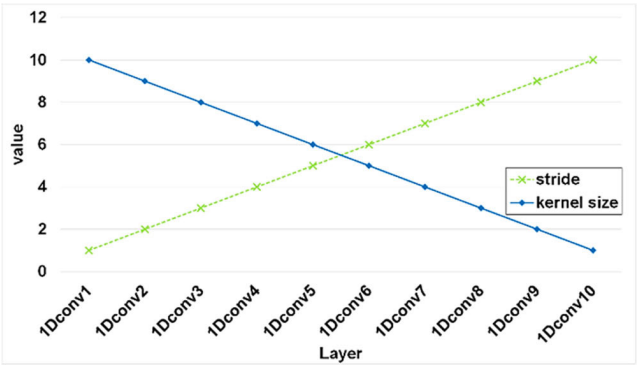

FIGURE 3. Differences in kernel size and stride for each layer of 1D-CNN architecture.

The output values processed in parallel by each 1D convolutional layer generate a single feature map through GMP processing, and they are combined with the values obtained from the VGGNet through the concatenate layer, as shown in Fig. 4.

The ensemble CNN model proposed in this paper uses two concatenate layers. To connect several feature maps output by each 1D CNN in the parallel structure as one feature map, the output of each layer is GMP processed. The GMP-processed data are then integrated by the first concatenate layer. The second concatenate layer combines the feature data obtained through the VGGNet and the data generated by the first concatenate layer. Here, the VGGNet data subjected to integration denote the data generated by converting the feature map obtained from the final convolutional layer of the VGGNet into 1D data via the flattened layer.

The data generated through the two concatenate layers are connected to the dropout and fully connected layers. The three dropout layers added between the layers of the networks to prevent overfitting in the learning process are set to 0.2 for A and 0.5 for both B and C, as depicted in Fig. 4. The first fully connected layer (FCL) displayed in Fig. 4 consists

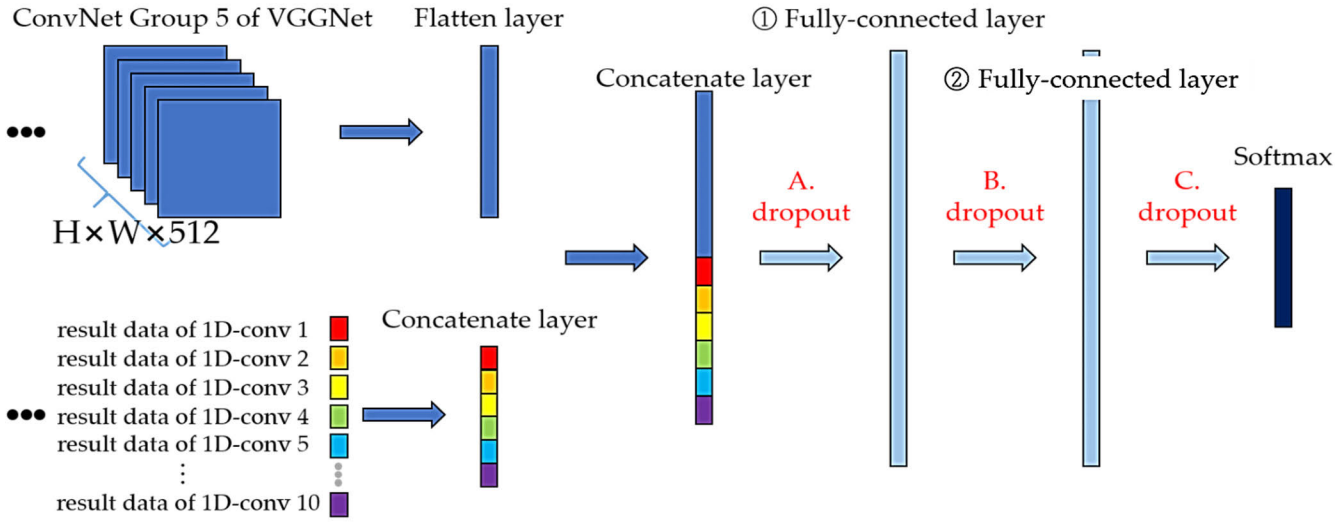

FIGURE 4. The structure of a neural network model for Alzheimer's diagnosis, connecting two convolutional models.

of 4,096 nodes, and it uses the ReLU activation function. The second FCL also uses 4,096 nodes but does not use an activation function. This configuration indicates that the first FCL optimizes non-linear classification using the ReLU function, and the second FCL performs linear classification to achieve an optimal learning effect. Finally, the data produced through all layers of the ensemble CNN predict one of the four AD stages for the output through the softmax() function.

The proposed ensemble CNN uses the adaptive gradient (Adagrad) optimizer as the optimization algorithm for learning data.

Adagrad is an improved version of the stochastic gradient descent optimizer and is a method capable of adjusting the learning rate according to the number of weight changes. When the weight changes frequently, this method assumes it is close to the optimal value and adjusts learning with a small learning rate to identify a fine optimal value. Conversely, if the weight changes less frequently, this method increases the learning rate rapidly to reduce the loss value and ensure high accuracy [55]. Equation (2) presents the formula for calculating the learning rate based on changes in the weight of a general Adagrad optimizer [55].

$$G_t = G_{t-1} + \left(\frac{\partial}{\partial W_t} L(t)\right)^2 = \sum_{i=0}^{t} \left(\frac{\partial L(i)}{\partial W_i}\right)^2$$
$$W_{t+1} = W_t - \frac{\alpha}{\sqrt{G_t + \varepsilon}} \cdot \frac{\partial}{\partial W_t} L(t) \quad (2)$$

The variable G_t in Equation (2) denotes the Adagrad optimizer at step t, and the square of the gradient ($\partial L/\partial W$) of the weight W_t for the current loss function $L(t)$ is added to the previous G_{t-1}. This represents the sum of squares for all gradients in each step. W_t denotes the weight vector at step t, ϵ is a very small constant used to prevent division by zero, and α is the learning rate.

IV. PERFORMANCE EVALUATION

A. MRI BRAIN DATASETS

MRI brain images collected from the open-source platform Kaggle were used as the AD dataset to evaluate the performance of the model proposed in this paper [56].

This dataset consisted of 6,400 MRI images with a resolution of 176 × 208 pixels that have been classified into four classes—Mild (MID), Moderate Demented (MOD), Non-Demented (ND), and Very Mild Demented (VMD)—as indicated in Fig. 5. Fig. 5 (a) presents an ND image, Fig. 5 (b) depicts a VMD image, Fig. 5 (c) presents an MID image, and Fig. 5 (d) presents an MD image. Table 3 presents the number of images for each class.

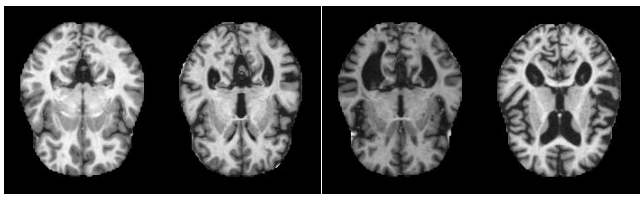

FIGURE 5. A class example of an MRI datasets for diagnosing Alzheimer's disease. (a) Non-Demented, (b) Very Mild Demented, (c) Mild Demented, (d) Moderate Demented.

TABLE 3. MRI dataset distribution.

No.	Class	No of Images
0	Non-Demented (ND)	3,200
1	Very Mild Demented (VMD)	2,240
2	Mild Demented (MID)	896
3	Moderate Demented (MD)	64

When examining each AD class image, image (a) reveals that black areas are sparsely distributed throughout the brain. As the AD stage progresses gradually, the black areas

increase in number. In addition, the contours of the brain appear gradually eroded inward.

As indicated in Table 3, the dataset consists of 3,200 ND images, 2,240 VMD images, 896 MID images, and 64 MD images. For each class, 80% of the data were used for training, and 20% were used as test data.

B. EXPERIMENTAL ENVIRONMENT

All experiments in this study were conducted in the following hardware environment: Windows 10 64-bit O/S, Intel Core i7-6700 CPU, 16 GB RAM, and NVIDIA GeForce GTX 2080 11 GB. To facilitate the functioning of the proposed model, the following software environment was used: Keras 2.3.1, Tensorflow-gpu2.0.0, NumPy 1.18.1, OpenCV-Python 4.2, and Scikit-image0.16.2. In addition, training was conducted using the early stopping function in all experiments, and the batch size was set to 32.

C. PERFORMANCE VERIFICATION BY COMPARISON WITH PREVIOUS CNN MODEL

To verify the performance of the proposed ensemble CNN model, we conducted comparative experiments with the following representative CNN models: VGGNet (16, 19) and AlexNet models. Table 4 summarizes the performance verification results according to the input image size for the proposed model.

TABLE 4. Performance verification results by input image size.

Input Size	Model	Precision	Recall	Accuracy	Loss
176×208	VGG-16	0.38	0.41	0.680	0.7660
	VGG-19	0.62	0.43	0.714	0.7307
	AlexNet	0.83	0.84	0.834	0.6502
	Our Model	*0.99*	*0.98*	*0.980*	*0.0681*
224×224	VGG-16	0.90	0.92	0.903	0.4806
	VGG-19	0.95	0.95	0.937	0.3568
	AlexNet	0.90	0.77	0.830	0.7040
	Our Model	*0.96*	*0.97*	*0.963*	*0.2130*
128×128	VGG-16	0.93	0.89	0.891	0.4630
	VGG-19	0.96	0.92	0.937	0.2534
	AlexNet	0.98	0.88	0.904	0.3726
	Our Model	*0.99*	*0.99*	*0.986*	*0.0518*
256×256	VGG-16	0.97	0.95	0.958	0.2573
	VGG-19	0.95	0.95	0.938	0.2324
	AlexNet	0.79	0.74	0.761	0.9114
	Our Model	***0.99***	***0.99***	***0.986***	***0.0385***
512×512	VGG-16	0.98	0.98	0.975	0.2437
	VGG-19	0.96	0.94	0.948	0.3277
	AlexNet	0.24	0.27	0.509	1.006
	Our Model	0.98	0.98	0.980	0.0744

The following five different sizes of input images were defined to conduct five experiments: 176 × 208, which is the size of the original image; 224 × 224, which is the default input size of the model; and three arbitrarily defined sizes of 128 × 128, 256 × 256, and 512 × 512. The results of the experiments revealed that the accuracy increased for the VGG-16 and VGG-19 models as the input image size increased. The AlexNet demonstrated the highest accuracy when the smallest input image size (128 × 128) was used.

In the 176 × 208 image size experiment, the proposed model achieved the highest accuracy of 0.980. The proposed model also outperformed other comparison models in terms of the precision (0.99) and recall (0.98). In the 224 × 224 image size experiment, the proposed model again had the highest accuracy of 0.963. This result indicates that the accuracy of the proposed model in this case was 0.017 lower than its accuracy in the original image size (176 × 208) experiment. Furthermore, the precision (0.03 lower) and recall (0.01 lower) also presented slight performance degradation.

In the 128 × 128 image size experiment, the accuracy performance results were as follows: the proposed model (0.986), VGG-19 model (0.937), AlexNet model (0.904), and VGG-16 model (0.891). Hence, the proposed model achieved the best performance. This result is the same as the result of the 256 × 256 image size experiment. In both experiments, the proposed model had an accuracy of 0.986. However, for the loss performance results, the proposed model had a loss of 0.0518 in the 128 × 128 image size experiment and a loss of 0.0385 in the 256 × 256 image size experiment. Hence, the 256 × 256 image size experiment resulted in a lower loss.

In the 512 × 512 image size experiment, the proposed model (0.980) achieved the highest accuracy; however, it only presented a slight difference of 0.05 compared to the VGG-16 model (0.975). The comparison experiments with existing CNN models verified that the proposed model maintained high accuracy, precision, and recall regardless of the size of the image. Based on these experiments, we confirm that the performance of the proposed model does not vary according to the size of the image.

This result can be attributed to the fact that the experiments used the data computed by the LFA algorithm. As stated, LFA data can record strong features regarding the shape of an object by analyzing the type of line segments and generating reduced data. Hence, the proposed model can obtain features that are stronger than the features collected by another 2D CNN model. Therefore, the proposed model can focus on collecting more distinguishable features in the learning process compared to the 2D CNN model. Furthermore, the shape features can be carefully observed using the 1D CNN, as in the proposed model; hence, the computed information is combined to yield excellent performance. Moreover, the performance of the proposed model does not vary according to the size of the input image.

Fig. 6 presents confusion matrix results corresponding to the validation experiment of the proposed model. The proposed model achieved good performance in all matrix results and presented stable performance in diagnosing early-

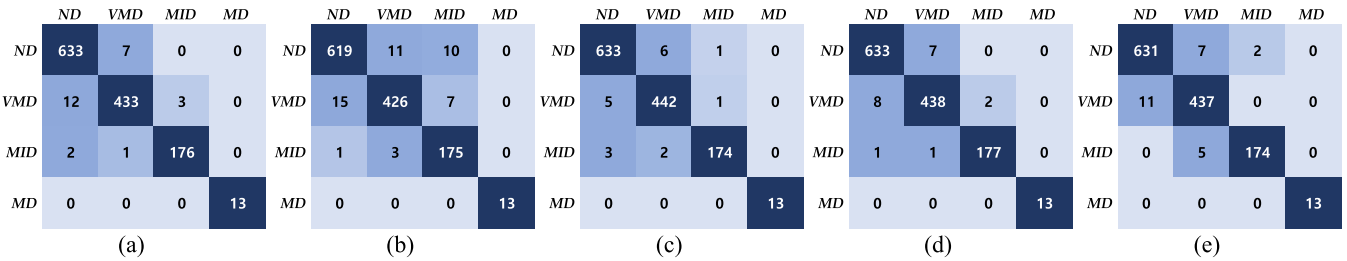

FIGURE 6. Confusion matrix results of the proposed model by input image size; (a) 176 × 208, (b) 224 × 224, (c) 128 × 128, (d) 256 × 256, (e) 512 × 512.

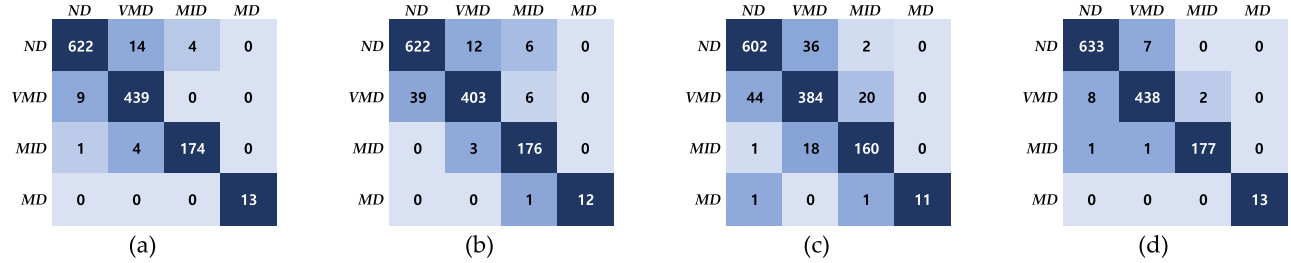

FIGURE 7. Comparative model confusion matrix results; (a) VGG-16 (512 × 512), (b) VGG-19 (512 × 512), (c) AlexNet (128 × 128), (d) Our Model (256 × 256).

stage AD. Fig. 7 presents confusion matrix results for the experiment in which the proposed model achieved the best performance in comparison with the other models. Even for the accuracy of each class in the confusion matrix, our proposed model outperformed the comparison models in the early stages of AD. Furthermore, the proposed model also achieved good performance at each AD stage. Hence, we confirmed that the proposed model demonstrated superior performance.

D. EXPERIMENTAL RESULTS AND DISCUSSION OF THE PROPOSED MODEL

Through this experiment, it was observed that improving the performance of existing single-image-based AD diagnostic models (VGG-16/19, AlexNet) is challenging. However, the potential to enhance the performance of AD diagnostic models by utilizing composite data has been demonstrated. In this paper, the LFA algorithm was employed to generate composite data. LFA data utilize only object shape information and can extract strong features related to lines through simple operations, making it suitable for utilizing additional data in AD diagnosis related to changes in brain shape.

Various experimental environments were constructed by adjusting the image size, and the obtained results are similar to those shown in Table 4. While it was confirmed that the proposed method outperforms in various conditions, performance degradation and improvement were observed with changes in image size. We believe that the reasons for performance degradation can be attributed to fluctuations in image size and the contour detection process of the LFA method. In this study, image enlargement was performed, which resulted in distortion of lines due to pixel rearrangement and interpolation during the enlargement process. Inappropriate changes in image size result in the loss of object proportions, causing shapes of lines, such as diagonals, to be distorted and recognized as curves. This distortion leads to changes in LFA data, ultimately impacting performance. Furthermore, while LFA data are created mainly based on types of lines, allowing the model training process to focus more heavily on features related to object shapes, this can also lead to a tendency to disregard other feature information, potentially causing performance degradation. To analyze this, further experiments with varying image size and the design of a method to preserve luminance and contrast features while learning must be considered.

Additionally, the structure of the existing AlexNet was designed with 10 parallel-connected 1D convolutional layers to minimize training time and model complexity. However, a comparison of performance and complexity with large-scale neural models needs to be conducted.

E. PERFORMANCE EVALUATION BY COMPARISON WITH PREVIOUS RELATED WORKS

The next experiment was conducted to compare the performance of the model proposed in this paper with that of models proposed in previous studies using the same dataset. Table 5 summarizes the performance of the DEMNET model proposed by Murugan et al. [37] and that of the KNN, SVC, and Xboost models presented by Kamal et al. [57]. In Table 5, AUG stands for image augmentation, ACC denotes accuracy, PR denotes precision, REC denotes recall, and FS denotes F1-score.

Notably, the dataset used in the experiment was imbalanced, as indicated in Table 3. The image augmentation method was thus used to solve this problem. In [37], the

TABLE 5. Results of performance comparison with prior literature.

Ref	Model	AUG	ACC	PR	REC	FS
[37]	DEMNET	*No*	0.85	0.80	0.88	0.83
	DEMNET	*Yes*	0.95	0.96	0.95	0.95
[57]	KNN	*No*	0.64	0.63	0.63	0.62
	SVC	*No*	0.82	0.81	0.81	0.82
	Xboost	*No*	0.77	0.76	0.76	0.75
-	Our Model	*No*	0.98	0.99	0.99	0.99

authors used this image augmentation method to eliminate the imbalance of datasets and quantified the performance based on the DEMNET model. In this case, the ACC was 0.95 in the experiment with AUG, and this accuracy was 0.1 higher than that in the experiment with no AUG. The PR, PRE, and FS values also presented improved results. However, the ensemble model proposed in this paper presented an ACC of 0.98 even when the AUG was not applied, and this performance result is superior to that of models proposed in previous studies. The results of the experiment indicated that the performance of the proposed ensemble model remained almost unchanged with changes in the input image size of the model. Moreover, the proposed model outperformed other existing models. The proposed model also demonstrated superior performance in terms of the loss, precision, and recall categories and exhibited stable classification performance even with imbalanced input data.

Moreover, the observed results were obtained because the proposed model was designed to analyze integrated information through two models rather than collecting several features using one model. The 1D CNN model, which uses the LFA features, carefully observes the shapes of the objects, and the VGGNet, which uses images, analyzes image features besides the shapes. Hence, overfitting and bias in the training data, which can occur when using one model, are prevented to enable stable learning.

V. DISCUSSION AND CONCLUSION

In this paper, we propose an ensemble CNN model for early diagnosis of AD by connecting a 2D CNN model and a 1D CNN model. This model is used to classify various stages of AD. To obtain input data for the 1D CNN model, the LFA algorithm is applied, transforming visual data into vector-type signal data. This process involves analyzing line segment types of objects within images and reducing data based on shape-centered approach. The data generated through this process captures strong features based on object shapes, making it easy to classify.

Furthermore, by training the proposed parallel 1D CNN, fine features corresponding to changes in line segments can be recognized. Additionally, the proposed model integrates features of the original image using the VGGNet model, thereby outperforming existing models. Through performance verification experiments using VGG-16/19 and AlexNet models, as well as comparison experiments with models proposed in previous studies on the same dataset, the proposed ensemble model exhibited superior performance with an accuracy of 0.986 and a loss of 0.0385. Therefore, we expect the proposed ensemble CNN model to yield excellent results in the field of MRI-based AD diagnosis.

Moreover, the proposed ensemble CNN model could introduce a new paradigm enhancing stability and reliability in early AD diagnosis research. However, variations in image size resulted in observed performance degradation and enhancement. Performance degradation arises from changes in image size and the outline detection process of the LFA method, and image enlargement introduced distortions. While LFA data emphasizes features related to object shapes, it may lead to performance degradation due to neglect of other feature information. More experiments involving variations in image size and considering methods to preserve luminance characteristics during training are necessary for analysis. Additionally, a comparison of performance and complexity with large-scale neural models is needed to validate the design of adding 10 parallel convolutional layers to the existing AlexNet architecture.

REFERENCES

[1] G. Lalli, J. M. Schott, J. Hardy, and B. De Strooper, "Aducanumab: A new phase in therapeutic development for Alzheimer's disease?" *EMBO Mol. Med.*, vol. 13, no. 8, 2021, Art. no. e14781.

[2] C. P. Ferri, M. Prince, C. Brayne, H. Brodaty, L. Fratiglioni, M. Ganguli, K. Hall, K. Hasegawa, H. Hendrie, Y. Huang, A. Jorm, C. Mathers, P. R. Menezes, E. Rimmer, and M. Scazufca, "Global prevalence of dementia: A delphi consensus study," *Lancet*, vol. 366, no. 9503, pp. 2112–2117, Dec. 2005.

[3] C. Wee, P. Yap, and D. Shen, "Prediction of Alzheimer's disease and mild cognitive impairment using cortical morphological patterns," *Hum. Brain Mapping*, vol. 34, no. 12, pp. 3411–3425, Dec. 2013.

[4] N. Zeng, H. Qiu, Z. Wang, W. Liu, H. Zhang, and Y. Li, "A new switching-delayed-PSO-based optimized SVM algorithm for diagnosis of Alzheimer's disease," *Neurocomputing*, vol. 320, pp. 195–202, Dec. 2018.

[5] M. Ewers, R. A. Sperling, W. E. Klunk, M. W. Weiner, and H. Hampel, "Neuroimaging markers for the prediction and early diagnosis of Alzheimer's disease dementia," *Trends Neurosciences*, vol. 34, no. 8, pp. 430–442, Aug. 2011.

[6] G. Nania, "World Alzheimer report," Tech. Rep., 2021.

[7] E. Nichols, C. E. Szoeke, S. E. Vollset, N. Abbasi, F. Abd-Allah, J. Abdela, M. T. E. Aichour, R. O. Akinyemi, F. Alahdab, S. W. Asgedom, and A. Awasthi, "Global, regional, and national burden of Alzheimer's disease and other dementias, 1990–2016: A systematic analysis for the global burden of disease study 2016," *Lancet Neurol.*, vol. 18, no. 1, pp. 88–106, Jan. 2019.

[8] L. Jia, Y. Du, and L. Chu, "Prevalence, risk factors, and management of dementia and mild cognitive impairment in adults aged 60 years or older in China: A cross-sectional study," *Lancet Public Health*, vol. 5, no. 12, pp. 661–671, 2020.

[9] Q. Cao, C. C. Tan, W. Xu, H. Hu, X. P. Cao, Q. Dong, L. Tan, and J. T. Yu, "The prevalence of dementia: A systematic review and metaanalysis," *J. Alzheimer's Disease*, vol. 73, no. 3, pp. 1157–1166. 2020.

[10] F. E. Matthews, A. Arthur, L. E. Barnes, J. Bond, C. Jagger, L. Robinson, and C. Brayne, "A two-decade comparison of prevalence of dementia in individuals aged 65 years and older from three geographical areas of England: Results of the cognitive function and ageing study I and II," *Lancet*, vol. 382, no. 9902, pp. 1405–1412, Oct. 2013.

[11] G. M. Savva, J. Zaccai, F. E. Matthews, J. E. Davidson, I. McKeith, and C. Brayne, "Prevalence, correlates and course of behavioural and psychological symptoms of dementia in the population," *Brit. J. Psychiatry*, vol. 194, no. 3, pp. 212–219, Mar. 2009.

[12] K. M. Langa, E. B. Larson, J. H. Karlawish, D. M. Cutler, M. U. Kabeto, S. Y. Kim, and A. B. Rosen, "Trends in the prevalence and mortality of cognitive impairment in the United States: Is there evidence of a compression of cognitive morbidity?" *Alzheimer's Dementia*, vol. 4, no. 2, pp. 134–144, Mar. 2008.

[13] C. Qiu, E. von Strauss, L. Backman, B. Winblad, and L. Fratiglioni, "Twenty-year changes in dementia occurrence suggest decreasing incidence in central Stockholm," *Sweden. Neurol.*, vol. 80, no. 20, pp. 1888–1894. 2013.

[14] P. Hudomiet, M. D. Hurd, and S. Rohwedder, "Dementia prevalence in the United States in 2000 and 2012: Estimates based on a nationally representative study," *J. Gerontol., Ser. B*, vol. 73, pp. 10–19, Apr. 2018.

[15] K. M. Langa, E. Larson, E. M. Crimmins, J. Faul, D. Levine, M. Kabeto, and D. Weir, "A comparison of the prevalence of dementia in the United States in 2000 and 2012," *Innov. Aging*, vol. 1, p. 933, Jul. 2017.

[16] V. A. Freedman, J. D. Kasper, B. C. Spillman, and B. L. Plassman, "Short-term changes in the prevalence of probable dementia: An analysis of the 2011–2015 national health and aging trends study," *J Gerontol., Ser. B*, vol. 73, no. 1, pp. 48–56, 2018.

[17] P. Wiberg, M. Waern, E. Billstedt, S. Östling, and I. Skoog, "Secular trends in the prevalence of dementia and depression in Swedish septuagenarians 1976–2006," *Psychol. Med.*, vol. 43, no. 12, pp. 2627–2634, Dec. 2013.

[18] K. D. Kochanek, J. Xu, and E. Arias, "Mortality in the United States," *NCHS Data Brief.*, vol. 395, pp. 1–8, Mar. 2020.

[19] *Alzheimer's Association Report, 2021 Alzheimer's Disease Facts and Figures, Alzheimers Dement*, 2021.

[20] G. Lalli, M. Rossor, J. B. Rowe, and B. De Strooper, "The dementia UK ecosystem: A call to action," *Lancet Neurol.*, vol. 20, no. 9, pp. 699–700, Sep. 2021.

[21] A. Burns and R. Howard, "COVID-19 and dementia: A deadly combination," *Int. J. Geriatr. Psychiatry*, vol. 36, no. 7, pp. 1120–1121, 2021.

[22] T. Ninomiya, "Study on the future projection of the elderly population with dementia in Japan," Health and Labor Sciences Research Grants, Special Health and Labor Sciences Research Project 2014 Research Report, Tech. Rep., 2015.

[23] T. Koyama, M. Sasaki, and H. Hagiya, "Place of death trends among patients with dementia in Japan: A population-based observational study," *Sci. Rep.*, vol. 9, p. 20235, Dec. 2019.

[24] J.-W. Jang, J. H. Park, S. Kim, S.-H. Lee, S.-H. Lee, and Y.-J. Kim, "Prevalence and incidence of dementia in South Korea: A nationwide analysis of the national health insurance service senior cohort," *J. Clin. Neurol.*, vol. 17, no. 2, pp. 249–256, 2021.

[25] R. Ren, J. Qi, S. Lin, X. Liu, and P. Yin, "The China Alzheimer report 2022," *Gen. Psychiatr.*, vol. 35, no. 1, pp. 1–19, 2022.

[26] World Health Organization. *Fact Sheet: Dementia*. Accessed: Oct. 1, 2022. [Online]. Available: http://www.who.int/en/news-room/fact-sheets/detail/dementia

[27] Alzheimer's Disease International. (2019). *World Alzheimer Report 2021*. Accessed: Sep. 21, 2021. [Online]. Available: https://www.alzint.org/resource/world-alzheimer-report-2021/

[28] K. Oh, Y.-C. Chung, K. W. Kim, W.-S. Kim, and I.-S. Oh, "Classification and visualization of Alzheimer's disease using volumetric convolutional neural network and transfer learning," *Sci. Rep.*, vol. 9, no. 1, pp. 1–16, Dec. 2019.

[29] Ministry of Health and Welfare. (2018). *Prevalence of Dementia in 2016*. Ministry of Health and Welfare, Seoul, (South) Korea. Accessed: Sep. 22, 2022. [Online]. Available: https: https://www.mohw.go.kr/eng/

[30] G. Chetelat and J.-C. Baron, "Early diagnosis of Alzheimer's disease: Contribution of structural neuroimaging," *NeuroImage*, vol. 18, no. 2, pp. 525–541, Feb. 2003.

[31] C.-M. Kim, R. C. Park, and E. J. Hong, "Breast mass classification using eLFA algorithm based on CRNN deep learning model," *IEEE Access*, vol. 8, pp. 197312–197323, 2020.

[32] C.-M. Kim, E. J. Hong, K. Chung, and R. C. Park, "Driver facial expression analysis using LFA-CRNN-based feature extraction for health-risk decisions," *Appl. Sci.*, vol. 10, no. 8, p. 2956, Apr. 2020.

[33] C.-M. Kim, E. J. Hong, K. Chung, and R. C. Park, "Line-segment feature analysis algorithm using input dimensionality reduction for handwritten text recognition," *Appl. Sci.*, vol. 10, no. 19, pp. 6904–6921, Oct. 2020.

[34] E. Hosseini-Asl, G. L. Gimel'farb, and A. El-Baz, "Alzheimer's disease diagnostics by a deeply supervised adaptable 3D convolutional network," Jul. 2016, *arXiv:1607.00556*.

[35] J. Venugopalan, L. Tong, H. R. Hassanzadeh, and M. D. Wang, "Multimodal deep learning models for early detection of Alzheimer's disease stage," *Sci. Rep.*, vol. 11, no. 1, pp. 1–13, Feb. 2021.

[36] S. Basaia, F. Agosta, L. Wagner, E. Canu, G. Magnani, R. Santangelo, and M. Filippi, "Automated classification of Alzheimer's disease and mild cognitive impairment using a single MRI and deep neural networks," *NeuroImage, Clin.*, vol. 21, Jan. 2019, Art. no. 101645.

[37] S. Murugan, C. Venkatesan, M. G. Sumithra, X.-Z. Gao, B. Elakkiya, M. Akila, and S. Manoharan, "DEMNET: A deep learning model for early diagnosis of Alzheimer diseases and dementia from MR images," *IEEE Access*, vol. 9, pp. 90319–90329, 2021.

[38] K. Simonyan and A. Zisserman, "Very deep convolutional networks for large-scale image recognition," in *Proc. 3rd Int. Conf. Learn. Represent. (ICLR)*, 2015, pp. 1–14.

[39] S. Lu, K. Xia, and S.-H. Wang, "Diagnosis of cerebral microbleed via VGG and extreme learning machine trained by Gaussian map bat algorithm," *J. Ambient Intell. Humanized Comput.*, vol. 14, no. 5, pp. 5395–5406, Feb. 2020, doi: 10.1007/s12652-020-01789-3.

[40] D. Hong, Y.-Y. Zheng, Y. Xin, L. Sun, H. Yang, M.-Y. Lin, C. Liu, B.-N. Li, Z.-W. Zhang, J. Zhuang, M.-Y. Qian, and S.-S. Wang, "Genetic syndromes screening by facial recognition technology: VGG-16 screening model construction and evaluation," *Orphanet J. Rare Diseases*, vol. 16, no. 1, pp. 1–8, Dec. 2021.

[41] U. Anusri, G. Dhatchayani, Y. Princely Angelinal, and S. Kamalraj, "An early prediction of Parkinson's disease using facial emotional recognition," *J. Phys., Conf.*, vol. 1937, no. 1, Jun. 2021, Art. no. 012058.

[42] H. A. Helaly, M. Badawy, and A. Y. Haikal, "Deep learning approach for early detection of Alzheimer's disease," *Cogn. Comput.*, vol. 14, pp. 1711–1727, Nov. 2021, doi: 10.1007/s12559-021-09946-2.

[43] D. Ebrahim, A. M. T. Ali-Eldin, H. E. Moustafa, and H. Arafat, "Alzheimer disease early detection using convolutional neural networks," in *Proc. 15th Int. Conf. Comput. Eng. Syst.*, Feb. 2021, pp. 1–6, doi: 10.1109/ICCES51560.2020.9334594.

[44] W. Yu, K. Yang, Y. Bai, T. Xiao, H. Yao, and Y. Rui, "Visualizing and comparing AlexNet and VGG using deconvolutional layers," in *Proc. 33rd Int. Conf. Mach. Learn.*, 2016, pp. 1–7.

[45] K. He, X. Zhang, S. Ren, and J. Sun, "Deep residual learning for image recognition," in *Proc. IEEE Conf. Comput. Vis. Pattern Recognit. (CVPR)*, Jun. 2016, pp. 770–778.

[46] C. Szegedy, W. Liu, Y. Jia, P. Sermanet, S. Reed, D. Anguelov, D. Erhan, V. Vanhoucke, and A. Rabinovich, "Going deeper with convolutions," in *Proc. IEEE Conf. Comput. Vis. Pattern Recognit. (CVPR)*, Boston, MA, USA, Jun. 2015, pp. 1–9.

[47] Y. LeCun, L. Bottou, Y. Bengio, and P. Haffner, "Gradient-based learning applied to document recognition," *Proc. IEEE*, vol. 86, no. 11, pp. 2278–2324, Nov. 1998.

[48] A. Krizhevsky, I. Sutskever, and G. E. Hinton, "Imagenet classification with deep convolutional neural networks," in *Proc. Adv. Neural Inf. Process. Syst. (NIPS)*, 2012, pp. 1097–1105.

[49] M. D. Zeiler and R. Fergus, "Visualizing and understanding convolutional networks," in *Proc. Eur. Conf. Comput. Vis.* Zurich, Switzerland: Springer, 2014, pp. 818–833.

[50] S. Kiranyaz, O. Avci, O. Abdeljaber, T. Ince, M. Gabbouj, and D. J. Inman, "1D convolutional neural networks and applications: A survey," *Mech. Syst. Signal Process.*, vol. 151, Apr. 2021, Art. no. 107398.

[51] W. Zhang, C. Li, G. Peng, Y. Chen, and Z. Zhang, "A deep convolutional neural network with new training methods for bearing fault diagnosis under noisy environment and different working load," *Mech. Syst. Signal Process.*, vol. 100, pp. 439–453, Feb. 2018.

[52] S. Kiranyaz, T. Ince, R. Hamila, and M. Gabbouj, "Convolutional neural networks for patient-specific ECG classification," in *Proc. 37th Annu. Int. Conf. IEEE Eng. Med. Biol. Soc. (EMBC)*, Aug. 2015, pp. 2608–2611.
[53] S. Kiranyaz, T. Ince, and M. Gabbouj, "Real-time patient-specific ECG classification by 1-D convolutional neural networks," *IEEE Trans. Biomed. Eng.*, vol. 63, no. 3, pp. 664–675, Mar. 2016.
[54] O. Avci, O. Abdeljaber, S. Kiranyaz, M. Hussein, and D. J. Inman, "Wireless and real-time structural damage detection: A novel decentralized method for wireless sensor networks," *J. Sound Vibrat.*, vol. 424, pp. 158–172, Jun. 2018.
[55] J. Duchi, E. Hazan, and Y. Singer, "Adaptive subgradient methods for online learning and stochastic optimization," *J. Mach. Learn. Res.*, vol. 12, pp. 2121–2159, Feb. 2011.
[56] S. Dubey. (2019). *Alzheimer's Dataset*. [Online]. Available: https://www.kaggle.com/tourist55/alzheimers-dataset-4-class-of-images
[57] M. S. Kamal, A. Northcote, L. Chowdhury, N. Dey, R. G. Crespo, and E. Herrera-Viedma, "Alzheimer's patient analysis using image and gene expression data and explainable-AI to present associated genes," *IEEE Trans. Instrum. Meas.*, vol. 70, pp. 1–7, 2021.

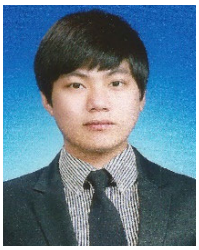

CHANG-MIN KIM received the B.S., M.S., and Ph.D. degrees from the Department of Computer Information Engineering, Sangji University, South Korea, in 2014 and 2022, respectively. Since 2023, he has been a Professor with the AI Software Education Institute, Soonchunhyang University, Asan-si, South Korea. His research interests include computer vision, databases, artificial networks, programming language, data mining artificial intelligence, machine learning, and deep learning.

WOOBEOM LEE received the B.S., M.S., and Ph.D. degrees in computer engineering from Yeungnam University, South Korea, in 1995, 1997, and 2000, respectively. Since 2000, he has been a Professor with the Department of Computer Engineering, Daegu Science University, and Yeungnam University, South Korea. He is currently a Professor with the Department of Information Communication Software Engineering, Sangji University. He services the Vice President of the Korean Convergence Signal Processing Society and has received several excellent paper awards at the society. His research interests include neuro-vision computing, deep learning, digital healthcare software, and IT convergence medical devices.